Mechanism of Aqueous Carbon Dioxide Reduction by the Solvated Electron

Rybkin, Vladimir V

DOI: https://doi.org/10.1021/acs.jpcb.0c07859

Mechanism of Aqueous Carbon Dioxide Reduction by the Solvated Electron

Vladimir V. Rybkin*

Department of Chemistry, University of Zurich, Winterthurerstrasse 190, Zurich 8057, Switzerland

E-mail: vladimir.rybkin@chem.uzh.ch

Phone: +41 44 63 54480

Abstract

Aqueous solvated electron, e^-_{aq}, a key species in radiation and plasma chemistry, can efficiently reduce CO_2 in a potential green chemistry application. Here, the mechanism of this reaction is unravelled by condensed-phase molecular dynamics based on the correlated wave function and an accurate DFT approximation. Here we design and apply the holistic protocol for solvated electron's reactions encompassing all relevant reaction stages starting from diffusion. The carbon dioxide reduction proceeds via a cavity intermediate, which is separated from the product, CO_2^-, by an energy barrier due to the bending of CO_2 and the corresponding solvent reorganization energy. The formation of the intermediate is caused by solvated electron's diffusion, whereas the intermediate transformation to CO_2^- is triggered hydrogen bond breaking in the second solvation shell of the solvated electron. This picture of activation-controlled e^-_{aq} reaction is very different from both rapid barrierless electron transfer, and proton-coupled electron transfer, where key transformations are caused by proton migration.

Graphical TOC Entry

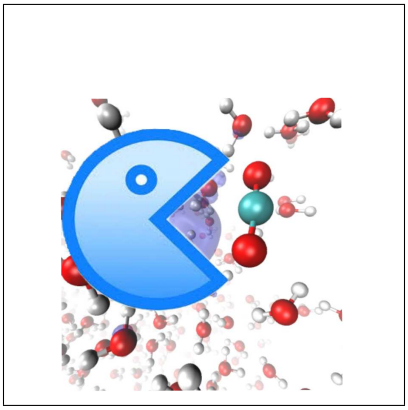

Keywords

solvated electrons, CO_2 reduction, many-body electronic structure theory, molecular dynamics, density functional theory

Introduction

The bulk hydrated electron, e^-_{aq},[1,2] is a key species in aqueous radiation[3] and plasma chemistry.[4] The structure of this non-standard species has long been elusive due to short life times and inaccessibility to direct structural methods. This opened opportunities for theory, although reliable modelling of e^-_{aq} is at least equally challenging as the corresponding experiments. Recent theoretical[5–8] contributions have set standards for reliable modelling of the bulk hydrated electron. These encompass condensed-phase *ab initio* molecular dynamics (AIMD) based on the second-order Møller-Plesset theory (MP2)[6,9] and hybrid exchange-correlation functional density functional theory (DFT).[5] MP2 provides accurate description of liquid water,[10] is free of delocalization error[11] pernicious for the description of radicals and is, moreover, a strict *ab initio* method, *i.e.* not based on empiricism and heuristic approximations. This comes at a price of extraordinary computational complexity, making such applications rare.[12] A computationally cheaper alternative is (DFT) based on hybrid exchange-correlation functional with a tuned amount of exact exchange[5] and non-local van der Waals correction.[13]

These methods can now be applied to the reactivity of e^-_{aq},[14–17] which feeds the interest to the species and introduces additional challenges. One of them is the preparation of realistic initial conditions. In particular, simulation should start with a well-defined cavity (to ensure the solvated rather pre-solvated state[7]), separated from the substrate. The published theoretical work on the reactivity of the bulk solvated electron is based on simpler approaches. Several studies involve dynamic cluster models rather than the condensed-phase ones.[18–20] Interesting *per se*, reaction mechanisms in clusters can be different from those in the bulk. In some articles substrates after electron attachments are simulated both in clusters[15,21,22] and in the condensed phase,[23,24] concentrating on relaxation kinetics, but omitting the diffusion and electron transfer. Finally, simple generalized gradient approximation (GGA) DFT[23–25] is applied for condensed-phase MD despite the delocalization error.

Here, we undertake an attempt to bring the simulation of solvated electron's reactivity

forward by performing AIMD with accurate electronic structure methods (hybrid functional DFT and MP) with the realistic molecular set-up. The reaction selected is CO_2 reduction by e^-_{aq} in high-temperature water. The process is not diffusion controlled and has a barrier of ca. 16 kJ/mol[26] of unknown nature. The barrier is, however, small enough to be able to "observe" the reaction in the non-biased MD simulations of moderate time scale accessible to computationally expensive electronic structure methods. Furthermore, interesting nuclear dynamics is expected due to the CO_2 structure change from linear to bent upon electron attachment.[27,28] The reaction is more than of methodological interest: it has been suggested for atmospheric carbon dioxide capture.[29,30] In addition, anion radical CO_2^- is often applied as a strong reducing agent[31] in plasma and radiation chemistry.

Computational Methods

Electronic structure calculations in the condensed-phase

Production AIMD

Production AIMD simulations were run based on DFT with hybrid exchange-correlation functional[32] and MP2 within spin-unrestricted formalism[33] as implemented in the CP2K program.[34] The core atomic levels were described with Goedecker-Teter-Hutter type pseudopotentials,[35] whereas triple-zeta quality basis sets were used for valence shells.[36,37]

Hybrid functional DFT calculations were done with the hybrid PBEh(50) functional, which combines PBE with 50% of exact exchange. The choice is motivated by the fact that the corresponding spin densities best approximate those from MP2.[6] Non-local van der Waals correction (rVV10) was applied to improve the description of intermolecular interactions.[13] This set-up is similar to the one optimized for the solvated electron in works.[5,7]

All calculations were performed under periodic boundary conditions and were restricted to $\Gamma-$point. The net charge of the unit cell introduced by the solvated electron was com-

pensated with a uniform background charge.

More details are given in the SI.

Constrained DFT calculations

Constrainded DFT (CDFT)[38] was applied to compute charge transfer energy, E_{CT}, between the cavity and the carbon dioxide molecule. In CDFT, diabatic states between which the electron is transferred are defined by constraints on the charge localization. E_{CT} is defined as the relaxation energy when the charge constraint is lifted. Here, one constraint was the CO_2 molecule, whereas the other included four water molecules forming the cavity. Although simplified, this setting proved to be instructive at the qualitative level.

CDFT calculations were performed for 50 of snapshots extracted from one of the PBEh(50)-rVV10 trajectories capturing the reactive event. The CP2K implementation of CDFT[39] was utilized with the same electronic structure set-up as for the production DFT AIMD trajectories. The Becke constraint for real space partitioning was applied.[40]

System preparation and molelcular dynamics

The system studied consists of 62 water molecules, a CO_2 molecule and an excess electron. The periodic cell size is $12.63 \times 12.63 \times 12.63$ Å, which corresponds to the experimental density of hot water at 373 K and normal pressure.

The system was prepared by equilibration in an NVT ensemble at 373 K (the temperature within the range of experimental measurements of Lisovskaya and Bartels *et al.*[26]) with a Cl^- anion instead of the excess electron to prevent the premature reaction, first with GGA DFT and then with hybrid PBEh(50)-rVV10. Chloride has been shown to form a solvation shell of similar size and shape as the one of the hydrated electron. Initial conditions for the production trajectories have been randomly selected from the equilibrated trajectory, chloride being substituted with an excess electron (*i. e.* chlorine nucleus removed). The initial distances between e^-_{aq} and CO_2 varied from 4 to 6 Å.

A total of 15 production trajectories have been run with hybrid DFT (PBEh(50)-rVV10) for either 2 ps or until the completion of the reaction in an NVE ensemble. Four production MP2 trajectories have been integrated. The intial conditions for the latter were taken from the production runs with hybrid DFT, leading to the products. Due to extreme computational cost they were integrated either until the reaction completion, or after one or several attempts to cross the barrier. More details are given in the SI.

Cluster models

Clusters containing CO_2 and four water molecules have been extracted from one of the reactive PBEh(50)-rVV10 trajectories. As Kumar *et al.* have suggested,[41] four water molecules in the solvation continuum are an accurate minimalistic model of the solvated electron. The reaction path was modelled by a series of constrained optimizations with fixed position of CO_2 corresponding to different bending angles. Geometry was relaxed with PBEh(50) functional with empirical D3 dispersion correction[42] and aug-PVDZ basis set,[43] proven to give accurate for the minimal model of the solvated electron.[41] The same has been done with MP2. In addition, single-point CCSD(T)[44] calculations have been performed at DFT-optimized geometries. Polarizable continuum model (PCM)[45] was applied for all calculations. Computations were performed with ORCA program.[46]

Structure classification

Structures evolving in AIMD have been classified by cluster analysis, *i.e.* unsupervised machine-learning approach, to avoid arbitrary assessments. Feature vectors used for clustering were based on the smooth-overlap of atomic positions (SOAP) descriptor[47,48] based exclusively on atomic positions. The SOAP matrix, characterizing the atomistic environment, was computed only for the carbon atom as the most relevant for the CO_2 reduction, and the three principal components of the SOAP matrix power spectrum were used as feature vectors.

The details are given in the SI.

Results and Discussion

Trajectory analysis

Cluster analysis of geometric structures allowed to divide the frames into four main structure types: separate reactants, intermediate, transition state (TS) region and the product, CO_2^-, shown in Figure 1. Initially CO_2 is randomly oriented with respect to the solvated electron's cavity as can be traced by the evolution of the carbon dioxide tilting angle (see Figures 2 and 3(b)). It is clearly seen from trajectory analysis that it is the solvated electron moving towards CO_2 during the diffusion stage. This is opposite to what is observed for the reaction between e^-_{aq} and hydronium,[18] but is expected based on the diffusion constant values: proton is one of the few species more mobile than solvated electron in water due to the Grotthus chain mechanism.[49]

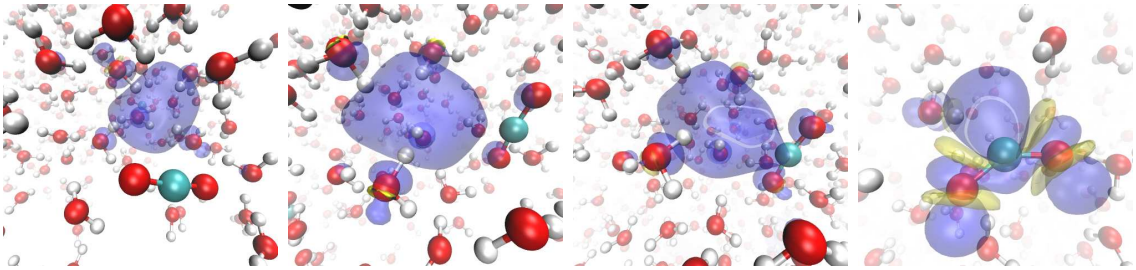

(a) Separated species: e^-_{aq} and CO_2 (b) Intermediate (c) Transition state region (d) Product: CO_2^-

Figure 1: Representative structures of different stages of CO_2 reduction by e^-_{aq} from an MP2 trajectory. Oxygen atoms are shown in red, hydrogen atoms in white, and carbon atoms in green. Spin density distribution isosurfaces are plotted in blue (positive) and yellow (negative) with isovalues of ± 0.001 a.u.

The intermediate is similar to the stable solvated electron's cavity (formed by either four or five water molecules), one water molecule being substituted with CO_2 (Figure 1(b)). Unlike H_2O it is not dipole oriented with the CO bonds towards the cavity, but tilted to the cavity surface at an angle of $100-120°$, due to the non-polar character of the bonds (Figures

2 3(b)). Gyration radius remains the same as in the neat aqueous cavity (Figure 3(a)) and CO_2 remains linear (Figure 3(b)). Transition region is characterized by the displacement of CO_2 towards the cavity center and the distortion of the nearly spherical spin density distribution, although the gyration radius remains unchanged (see Figures 1(c) and 3(a)). Finally, the product, CO_2^- is bent, whereas spin density distribution exhibits characteristic nodal structure with significant spin polarization and small gyration radius (see Figures 1(d) and 3(a)).

Structure classification based on cluster analysis generally meets chemical intuition. Some structures with collapsed cavity and bent CO_2^- are, however, assigned to the transition region (1.5 to 1.7 ps in Figure 2), seemingly counterintuitive. On the one hand, this may be an artifact of the unsupervised procedure, based on purely structural data. On the other hand, this may reflect fine changes in the structure evolution, not captured by direct human observation. In the absence of unequivocal criteria for configuration space partitioning, we deem the performance of cluster analysis based on the SOAP descriptor satisfactory and promising.

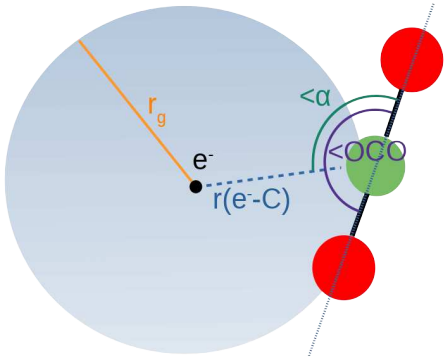

Figure 2: Collective variables: e^- - the center of the spin density distribution (of an excess electron); r_g - gyration radius of the spin density distribution; $r(e-C)$ - distance between e^- and the carbon atom; $\angle\alpha$ - tilting angle of CO_2; $\angle OCO$ - CO_2 bending angle.

The qualitative picture of the reaction dynamics is summarized in equation (1) and Table

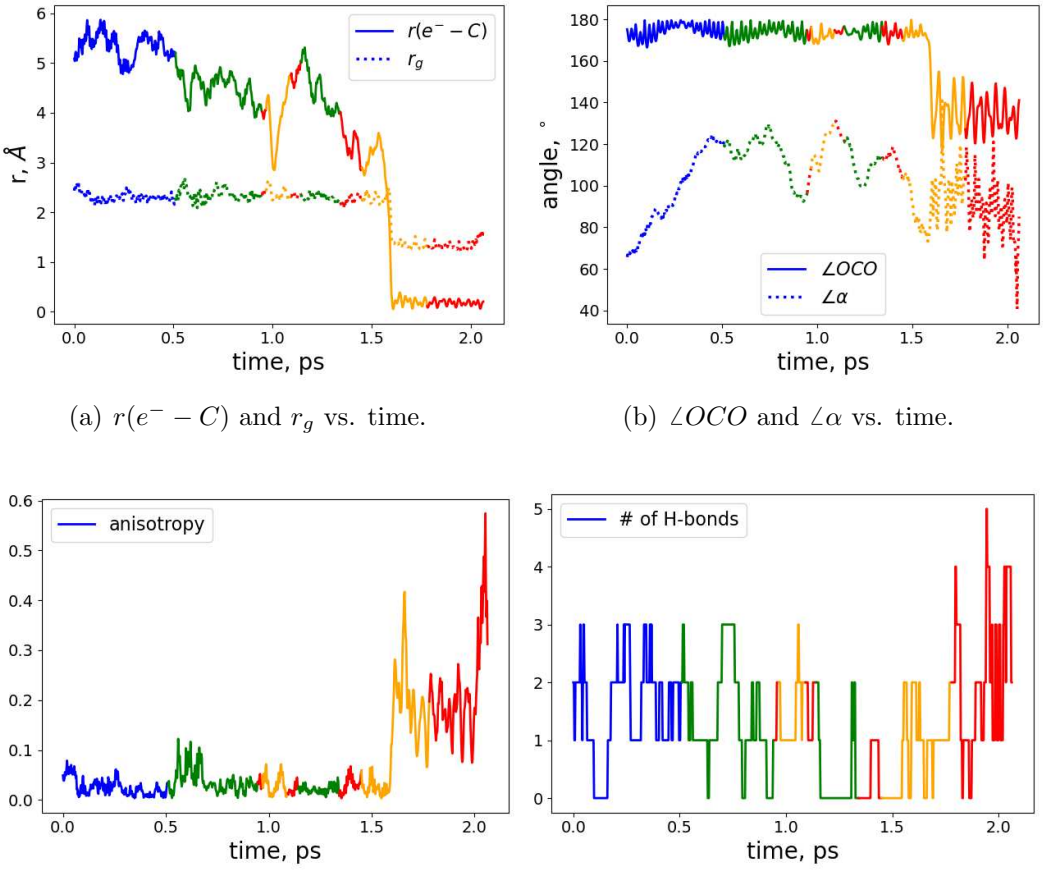

(a) $r(e^- - C)$ and r_g vs. time.

(b) $\angle OCO$ and $\angle\alpha$ vs. time.

(c) Spin distribution anisotropy vs. time.

(d) Number of hydrogen bonds of the relevant cavity-forming molecule

Figure 3: Time evolution of some collective variables along one of the reactive hybrid DFT trajectories. Colors correspond to the structure classification by cluster analysis: blue - separate reactants (diffusion stage); green - intermediate; orange - transition state region; red - products. The formation of the intermediate is characterized by reorientation of the CO_2 coming at a sharp angle ($\angle\alpha$), but taking the position at the cavity with the obtuse tilting angle. The reaction completion is marked by the bending of the CO_2 ($\angle OCO$), drop in gyration radius (r_g) and transfer of the spin density to CO_2 ($r(e^- - C) \to 0$) after 1.5 ps. An unsuccessful attempt to overcome the barrier takes place at ca. 1 ps.

1 (see also the video in the SI):

$$e^- + CO_2 \overset{diffusion}{\rightleftharpoons} e^- \cdot\cdot CO_2 \overset{barrier}{\rightleftharpoons} [e^- \cdot\cdot CO_2]^* \longrightarrow {CO_2}^- \quad (1)$$

Table 1: Trajectory outcomes. Number of unsuccessful attempts to cross the barrier is given in parentheses.

Method	Reactive	Non-reactive
PBEh(50)-rVV10	8(3)	7(4)
MP2	2(1)	2(2)

The intermediate shown in Figure 1(b) is formed via diffusion in all trajectories. Thus, we conclude that there is no barrier to the formation of the intermediate. Its lifetime can be up to 2 ps (limit of our time-scale) and is on average 0.5 ps. In approximately half of the trajectories it converts to the products and it two DFT trajectories it falls apart to form the isolated CO_2 and the solvated electron (Figure 1(a)). Thus, the intermediate must be a shallow local minimum.

The experimentally observed barrier is the one separating the intermediate and the products. Indeed, out of 15 observed attempts to form the product from the intermediate via the transition state (TS) region only eight lead to the products (denoted as reactive in Table 1) in case of DFT and two of four in case of MP2, *e.g.* ca. 50%. Note that before the reaction happens in the reactive trajectories, a few unsuccessful attempts to cross the barrier may take place: this happens in one of the two reactive MP2 trajectories and in three of eight DFT reactive trajectories. Unsuccessful crossing attempts are rapid as illustrated in Figure 2 (at 1 ps in the graph), indicating that the corresponding structures are not stable, *i.e.* correspond to the TS region. This picture is in sharp contrast to the predicted barrierless reduction of amide,[25] being complete in less than 0.5 ps without formation of intermediates.

Cluster vs. Bulk Models

In an attempt to calculate the reaction barrier, potential energy surface (PES) scans of the clusters have been performed as described in Subsection Cluster Models. Surprisingly, PES scans reveal no barrier (see the Figure in the SI) as CO_2 molecule is being bent, which is in contrast to the behavior observed in the bulk AIMD trajectories. At the same time, the transformation mechanism revealed for clusters is different to the one in the condensed-phase. Already at the CO_2 bending angle of 170° the cavity in the cluster is collapsed (see Figure 4): two-cavity forming water molecules form a hydrogen bonds. In the bulk, when the bending angle in CO_2 reaches 170° the cavity still exists, although it is distorted (marked by the increase in anisotropy as shown in Figure 3(c)). As shown in Figure 4), one of the water molecules coordinates to the oxygen atom of CO_2, although the hydrogen bond between one of its hydrogen atoms and the oxygen of CO_2 is not yet formed. In the bulk, cavity-forming molecules are bound to the second solvation shell by one or two hydrogen bonds (absent in the cluster). Those prevent the cavity from immediate collapse as soon as CO_2 bending angle reaches ca. 170°. In the minimalistic cluster model, such hindrance does not not exist and the cavity collapses with the slight bending of CO_2. The formed hydrogen bond network stabilizes the bent structure responsible for the barrier. Thus, a cluster model suitable for the CO_2 reduction must include the second solvation shell of the solvated electron (at least eight more water molecules). Static modelling of such extended clusters is challenging and not always instructive due to their flat PES. Importantly, the need for a larger cluster model is a retrospective knowledge, based on the already available information from condensed-phase simulations. However, even this may not be enough as recently shown by Park and Schwartz, who have come to the conclusion that dynamic behaviour of the the 16-water model with implicit solvent is closer to this of cluster-anions than to the bulk.[50]

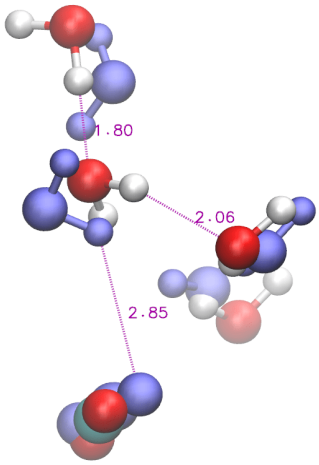

Figure 4: Comparison between cluster and bulk structures with CO_2 bending angle of 170°. The bulk structure (blue) is carved from the trajectory, whereas the cluster structure (red and white) is obtained from the bulk one by the constrained optimization with the fixed CO_2 fragment. Hydrogen bond network is formed in the cluster (bonds being shown in purple) leading to the cavity collapse. In the bulk, cavity exists and one of the water molecules (to the left) coordinates to CO_2; no hydrogen bonds between cavity-forming molecules have been formed.

Detailed Mechanism

Having recognized the importance of hydrogen bonding network in the second solvation shell, we were able to find out an event triggering the transformation of the intermediate: the thermal breaking of one or more hydrogen bonds with the second solvation shell one of the cavity-forming water molecules. This molecule is now bound by only one acceptor hydrogen bond (or even none) as shown in Figure 3(d): before the first (ca. 1 ps) and the second (ca. 1.5 ps) barrier-crossing attempts the molecule becomes non-hydrogen bonded. This weaker bound water molecule is then able to coordinate to CO_2 (see Figure 4). It transfers some charge favouring bending and distorting the cavity at the same time as marked by the increase in anysotropy (see Figure 3(c)). The cavity and the carbon dioxide molecule now compete for the charge. Charge transfer energy, E_{CT}, values plotted in Figure 5 favor electron binding to the cavity until CO_2 is bent to less than 170°. Then E_{CT} changes sign and the transformation is rapidly and irreversible takes place. The negative values of E_{CT} characteristic for the intermediate prove the existence of the barrier: the mere presence of CO_2 next to the solvated electron does not cause the reaction. However, the values of E_{CT} do not allow to compute the barrier size directly.

As hydrogen bond network is responsible for launching the reaction it also can revert barrier crossing: after 1 ps in Figure 3(d) the hydrogen bond network is being partially restored stabilizing the cavity and preventing charge transfer to CO_2.

Similar to the results of MD simulations on clusters,[20] electron transfer to CO_2 is followed (and facilitated) by hydrogen bond formation between CO_2^- and one or two cavity-forming molecules (see Figure 4). However, in the bulk liquid these bonds are destroyed within less than 100 fs. This is caused by cavitation. Indeed, the electron is transferred to CO_2 before the solvent is able to rearrange. As the now empty cavity collapses, the released energy pushes the CO_2^- away disrupting freshly formed hydrogen bonds.

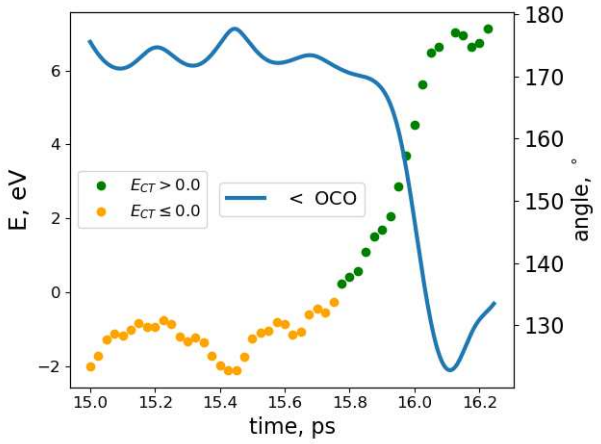

Figure 5: Charge transfer energies, E_{CT}, from the catity forming water molecules to CO_2 and the bending angle for one of the trajectories during the reactive event. Positive E_{CT} correspond to favorable electron binding to the carbon dioxide. Note the correlation between bending angle and E_{CT}.

Conclusions

Picosecond time-scale AIMD based on PBEh(50)-rVV10 and MP2 electronic structure theories reveal atomistic picture of aqueous carbon dioxide reduction by the solvated electron. The reaction proceeds via a distinct intermediate, where the CO_2 molecule is embedded in the solvated electron's cavity along with the four water molecules. The conversion of the intermediate to CO_2^- is triggered by hydrogen bond network fluctuations, *viz.* the bond breaking between one of the cavity forming water molecules and the second solvation shell. This allows the water molecule to coordinate to CO_2 and destabilizes the cavity, which now competes for the electron with carbon dioxide. Not every such attempt leads to the electron transfer: the intermediate may be restored and even dissociate to the separated CO_2 and e^-_{aq}. This happens when hydrogen bond network in the second solvation shell of the intermediate restores before the charge transfer is able to occur. Such behaviour together with picosecond time-scale of transformation and charge transfer energies is consistent with the existence of a small barrier of CO_2 reduction by the solvated electron, observed experimentally. After the electron transfer a curious manifestation of cavitation at the atomic scale is observed: the collapsing cavity pushes the CO_2 away from the reaction site and breaks freshly formed

hydrogen bonds.

The methodology applied here, hybrid DFT and MP2-driven condensed-phase AIMD starting from preformed cavity at a distance from the substrate, has proven to be promising. Indeed, it is able to unveil a rich atomistic picture of the reaction even with restricted statistics and at moderate time scales, covering all reaction stages from diffusion to the product relaxation and providing a qualitative behaviour consistent with the experiment.

Acknowledgement

This work has been supported by the Swiss National Science Foundation in the form of Ambizione grant No. PZ00P2_174227. This work was also supported by a grant from the Swiss National Supercomputing Centre (CSCS) under Project ID s976. The author is grateful to Dr. Marcella Iannuzzi and Dr. Yasmin S. Al-Hamdani (University of Zurich) from fruitful discussions.

Supporting Information Available

Further details of calculations and data analysis are given in the supported information. A video of the reactive MP2 trajectory is available as supplementary material.

References

(1) Herbert, J. M.; Coons, M. P. The Hydrated Electron. *Annual Review of Physical Chemistry* **2017**, *68*, 447–472, PMID: 28375692.

(2) Hart, E. J.; Boag, J. W. Absorption Spectrum of the Hydrated Electron in Water and in Aqueous Solutions. *Journal of the American Chemical Society* **1962**, *84*, 4090–4095.

(3) Garrett, B. C.; Dixon, D. A.; Camaioni, D. M.; Chipman, D. M.; Johnson, M. A.; Jonah, C. D.; Kimmel, G. A.; Miller, J. H.; Rescigno, T. N.; Rossky, P. J. et al. Role of Water in Electron-Initiated Processes and Radical Chemistry: Issues and Scientific Advances. *Chemical Reviews* **2005**, *105*, 355–390, PMID: 15720157.

(4) Rumbach, P.; Bartels, D. M.; Sankaran, R. M.; Go, D. B. The solvation of electrons by an atmospheric-pressure plasma. *Nature Communications* **2015**, *6*, 7248.

(5) Ambrosio, F.; Miceli, G.; Pasquarello, A. Electronic levels of excess electrons in liquid water. *The journal of physical chemistry letters* **2017**, *8*, 2055–2059.

(6) Wilhelm, J.; VandeVondele, J.; Rybkin, V. V. Dynamics of the Bulk Hydrated Electron from Many-Body Wave-Function Theory. *Angewandte Chemie International Edition* **2019**, *58*, 3890–3893.

(7) Pizzochero, M.; Ambrosio, F.; Pasquarello, A. Picture of Wet Electron: A Localized Transient State in Liquid Water. *Chemical Science* **2019**,

(8) Dasgupta, S.; Rana, B.; Herbert, J. M. Ab Initio Investigation of the Resonance Raman Spectrum of the Hydrated Electron. *The Journal of Physical Chemistry B* **2019**, *123*, 8074–8085, PMID: 31442044.

(9) Møller, C.; Plesset, M. S. Note on an Approximation Treatment for Many-Electron Systems. *Phys. Rev.* **1934**, *46*, 618–622.

(10) Del Ben, M.; Schönherr, M.; Hutter, J.; VandeVondele, J. Bulk Liquid Water at Ambient Temperature and Pressure from MP2 Theory. *The Journal of Physical Chemistry Letters* **2013**, *4*, 3753–3759.

(11) Mori-Sánchez, P.; Cohen, A. J.; Yang, W. Localization and Delocalization Errors in Density Functional Theory and Implications for Band-Gap Prediction. *Phys. Rev. Lett.* **2008**, *100*, 146401.

(12) Rybkin, V. V. Sampling Potential Energy Surfaces in the Condensed Phase with Many-Body Electronic Structure Methods. *Chemistry – A European Journal* **2019**, *26*, 362–368.

(13) Sabatini, R.; Gorni, T.; de Gironcoli, S. Nonlocal van der Waals density functional made simple and efficient. *Phys. Rev. B* **2013**, *87*, 041108.

(14) Anbar, M. *Solvated Electron*; Chapter 6, pp 55–81.

(15) Gu, J.; Leszczynski, J.; Schaefer, H. F. Interactions of Electrons with Bare and Hydrated Biomolecules: From Nucleic Acid Bases to DNA Segments. *Chemical Reviews* **2012**, *112*, 5603–5640, PMID: 22694487.

(16) Gordon, S.; Hart, E. J.; Matheson, M. S.; Rabani, J.; Thomas, J. K. Reactions of the hydrated electron. *Discuss. Faraday Soc.* **1963**, *36*, 193–205.

(17) Getoff, N. Possibilities on the radiation-induced incorporation of CO2 and CO into organic compounds. *International Journal of Hydrogen Energy* **1994**, *19*, 667 – 672.

(18) Marsalek, O.; Uhlig, F.; VandeVondele, J.; Jungwirth, P. Structure, Dynamics, and Reactivity of Hydrated Electrons by Ab Initio Molecular Dynamics. *Accounts of Chemical Research* **2012**, *45*, 23–32, PMID: 21899274.

(19) Kumar, A.; Adhikary, A.; Shamoun, L.; Sevilla, M. D. Do Solvated Electrons (eaq–)

Reduce DNA Bases? A Gaussian 4 and Density Functional Theory-Molecular Dynamics Study. *The Journal of Physical Chemistry B* **2016**, *120*, 2115–2123, PMID: 26878197.

(20) Breen, K. J.; DeBlase, A. F.; Guasco, T. L.; Voora, V. K.; Jordan, K. D.; Nagata, T.; Johnson, M. A. Bottom-Up View of Water Network-Mediated CO2 Reduction Using Cryogenic Cluster Ion Spectroscopy and Direct Dynamics Simulations. *The Journal of Physical Chemistry A* **2012**, *116*, 903–912, PMID: 22145700.

(21) Gu, J.; Xie, Y.; Schaefer, H. F. Near 0 eV Electrons Attach to Nucleotides. *Journal of the American Chemical Society* **2006**, *128*, 1250–1252, PMID: 16433542.

(22) Brezina, K.; Jungwirth, P.; Marsalek, O. Benzene Radical Anion in the Context of the Birch Reduction: When Solvation Is the Key. *The Journal of Physical Chemistry Letters* **0**, *0*, 6032–6038, PMID: 32628025.

(23) Wu, X.; Gao, L.; Liu, J.; Yang, H.; Wang, S.; Bu, Y. Excess electron reactivity in amino acid aqueous solution revealed by ab initio molecular dynamics simulation: anion-centered localization and anion-relayed electron transfer dissociation. *Phys. Chem. Chem. Phys.* **2015**, *17*, 26854–26863.

(24) Wu, X.; Gao, L.; Liu, J.; Yang, H.; Wang, S.; Bu, Y. Excess electron reactivity in amino acid aqueous solution revealed by ab initio molecular dynamics simulation: anion-centered localization and anion-relayed electron transfer dissociation. *Phys. Chem. Chem. Phys.* **2015**, *17*, 26854–26863.

(25) Zhang, R.; Bu, Y. Bifurcate localization modes of excess electron in aqueous Ca2+ amide solution revealed by ab initio molecular dynamics simulation: towards hydrated electron versus hydrated amide anion. *Phys. Chem. Chem. Phys.* **2016**, *18*, 18868–18879.

(26) Lisovskaya, A.; Bartels, D. M. Reduction of CO2 by hydrated electrons in high temperature water. *Radiation Physics and Chemistry* **2019**, *158*, 61 – 63.

(27) Janik, I.; Tripathi, G. N. R. The nature of the CO2- radical anion in water. *The Journal of Chemical Physics* **2016**, *144*, 154307.

(28) Rybkin, V. V.; VandeVondele, J. Nuclear Quantum Effects on Aqueous Electron Attachment and Redox Properties. *The Journal of Physical Chemistry Letters* **2017**, *8*, 1424–1428, PMID: 28296416.

(29) Rumbach, P.; Xu, R.; Go, D. B. Electrochemical Production of Oxalate and Formate from CO2by Solvated Electrons Produced Using an Atmospheric-Pressure Plasma. *Journal of The Electrochemical Society* **2016**, *163*, F1157–F1161.

(30) Zhang, L.; Zhao, Z.-J.; Wang, T.; Gong, J. Nano-designed semiconductors for electro- and photoelectro-catalytic conversion of carbon dioxide. *Chem. Soc. Rev.* **2018**, *47*, 5423–5443.

(31) Armstrong, D. A.; Huie, R. E.; Koppenol, W. H.; Lymar, S. V.; Merényi, G.; Neta, P.; Ruscic, B.; Stanbury, D. M.; Steenken, S.; Wardman, P. Standard electrode potentials involving radicals in aqueous solution: inorganic radicals (IUPAC Technical Report). *Pure and Applied Chemistry* **2015**, *87*, 1139 – 1150.

(32) Guidon, M.; Schiffmann, F.; Hutter, J.; VandeVondele, J. Ab initio molecular dynamics using hybrid density functionals. *The Journal of Chemical Physics* **2008**, *128*, 214104.

(33) Rybkin, V. V.; VandeVondele, J. Spin-unrestricted second-order Møller–Plesset (MP2) forces for the condensed phase: from molecular radicals to f-centers in solids. *Journal of chemical theory and computation* **2016**, *12*, 2214–2223.

(34) Kühne, T. D.; Iannuzzi, M.; Del Ben, M.; Rybkin, V. V.; Seewald, P.; Stein, F.; Laino, T.; Khaliullin, R. Z.; Schütt, O.; Schiffmann, F. et al. CP2K: An electronic structure and molecular dynamics software package - Quickstep: Efficient and accurate electronic structure calculations. *The Journal of Chemical Physics* **2020**, *152*, 194103.

(35) Goedecker, S.; Teter, M.; Hutter, J. Separable dual-space Gaussian pseudopotentials. *Phys. Rev. B* **1996**, *54*, 1703–1710.

(36) Del Ben, M.; Hutter, J.; VandeVondele, J. Electron Correlation in the Condensed Phase from a Resolution of Identity Approach Based on the Gaussian and Plane Waves Scheme. *Journal of Chemical Theory and Computation* **2013**, *9*, 2654–2671, PMID: 26583860.

(37) VandeVondele, J.; Hutter, J. Gaussian basis sets for accurate calculations on molecular systems in gas and condensed phases. *The Journal of Chemical Physics* **2007**, *127*, 114105.

(38) Kaduk, B.; Kowalczyk, T.; Van Voorhis, T. Constrained Density Functional Theory. *Chemical Reviews* **2012**, *112*, 321–370, PMID: 22077560.

(39) Holmberg, N.; Laasonen, K. Efficient Constrained Density Functional Theory Implementation for Simulation of Condensed Phase Electron Transfer Reactions. *Journal of Chemical Theory and Computation* **2017**, *13*, 587–601, PMID: 28009515.

(40) Becke, A. D. A multicenter numerical integration scheme for polyatomic molecules. *The Journal of Chemical Physics* **1988**, *88*, 2547–2553.

(41) Kumar, A.; Walker, J. A.; Bartels, D. M.; Sevilla, M. D. A Simple ab Initio Model for the Hydrated Electron That Matches Experiment. *The Journal of Physical Chemistry A* **2015**, *119*, 9148–9159, PMID: 26275103.

(42) Grimme, S.; Antony, J.; Ehrlich, S.; Krieg, H. A consistent and accurate ab initio parametrization of density functional dispersion correction (DFT-D) for the 94 elements H-Pu. *The Journal of Chemical Physics* **2010**, *132*, 154104.

(43) Dunning, T. H. Gaussian basis sets for use in correlated molecular calculations. I. The

atoms boron through neon and hydrogen. *The Journal of Chemical Physics* **1989**, *90*, 1007–1023.

(44) Raghavachari, K.; Trucks, G. W.; Pople, J. A.; Head-Gordon, M. Reprint of: A fifth-order perturbation comparison of electron correlation theories. *Chemical Physics Letters* **2013**, *589*, 37 – 40, SPECIAL NOBEL ISSUE.

(45) Mennucci, B. Polarizable continuum model. *WIREs Computational Molecular Science* **2012**, *2*, 386–404.

(46) Neese, F. The ORCA program system. *WIREs Computational Molecular Science* **2012**, *2*, 73–78.

(47) De, S.; Bartók, A. P.; Csányi, G.; Ceriotti, M. Comparing molecules and solids across structural and alchemical space. *Phys. Chem. Chem. Phys.* **2016**, *18*, 13754–13769.

(48) Himanen, L.; Jäger, M. O.; Morooka, E. V.; Canova, F. F.; Ranawat, Y. S.; Gao, D. Z.; Rinke, P.; Foster, A. S. DScribe: Library of descriptors for machine learning in materials science. *Computer Physics Communications* **2020**, *247*, 106949.

(49) Herbert, J. M. Structure of the aqueous electron. *Physical Chemistry Chemical Physics* **2019**, *21*, 20538–20565.

(50) Park, S. J.; Schwartz, B. J. Evaluating Simple Ab Initio Models of the Hydrated Electron: The Role of Dynamical Fluctuations. *The Journal of Physical Chemistry B* **0**, *0*, null, PMID: 33078930.